International Committee for Future Accelerators

Sponsored by the Particles and Fields Commission of IUPAP

Beam Dynamics Newsletter

No. 45

Issue Editor:
R. Wanzenberg

Editor in Chief:
W. Chou

April 2008

4.9 Geometrical Impedance of the PETRA III Damping Wiggler Section

Victor Smaluk, Budker Institute of Nuclear Physics, Novosibirsk, Russia
Rainer Wanzenberg, DESY, Notkestr. 85, Hamburg, Germany
Mail to: smaluk@inp.nsk.su

4.9.1 Introduction

For the PETRA III synchrotron radiation source [1], a damping wiggler section has been designed in the Budker Institute of Nuclear Physics. Two such sections will be installed to decrease the PETRA III beam emittance. The wiggler section vacuum chamber includes a set of synchrotron radiation absorbers intended to accept more than 200 kW of radiation power during the machine routine operation. An irregular cross-section of the vacuum chamber results in a quite large coupling impedance. To estimate the contribution of the wiggler section to the total PETRA III broad-band impedance, three-dimensional computer simulations of the wake fields have been performed using GdfidL code [2], in comparison with analytical formulae.

4.9.2 Collective Effects and Coupling Impedance

Particle dynamics of an intensive beam moving in a vacuum chamber differs from a single-particle dynamics. The beam induces quite strong electromagnetic fields (wake fields) affecting the beam itself. The most significant results of the collective effects are various instabilities of beam motion, which can lead to beam losses or beam quality deterioration.

In the time domain, beam-environment interaction is characterized by the wake potential defined as the wake force integrated along the beam trajectory over the interaction length [3]. In the frequency domain, each part of a vacuum chamber can be represented as frequency-dependent coupling impedance, which is the Fourier transform of the wake function. The real (resistive) part of the impedance leads to a particle energy loss, the imaginary (reactive) one leads to a shift of particle oscillation phase. Total impedance of a vacuum chamber is a sum of impedances of all its components.

For almost all practical cases, coupling impedance of a vacuum chamber component can be approximated by a resonant circuit for each oscillation mode:

$$Z_{\parallel}(\omega) = \frac{R_s}{1 + iQ\left(\frac{\omega}{\omega_r} - \frac{\omega_r}{\omega}\right)}, \qquad Z_{\perp}(\omega) = \frac{\omega_r}{\omega}\frac{R_s}{1 + iQ\left(\frac{\omega}{\omega_r} - \frac{\omega_r}{\omega}\right)}, \qquad (1)$$

where R_s is the shunt resistance of the longitudinal (Ω) or dipole transverse (Ω/m) mode, ω_r is the resonance frequency, and Q is the quality factor.

Because a damping (rising) time of an oscillation mode is $\tau = 2Q/\omega_r$, a high-Q (narrow-band) mode is more long-living than a low-Q (broad-band) one. Thus, for a whole vacuum chamber or any its component, the narrow-band impedance and the broad-band one can be separated (see Figure 1). However, this separation is not rigorous because we should take into account the beam oscillation bandwidth. It is more

realistic to consider the narrow-band or the broad-band impedance as a contribution to the beam-environment interaction within the impedance bandwidth rather than as the pure electromagnetic characteristics of the vacuum chamber component itself. Anyway we can assert that the narrow-band impedance leads to the bunch-by-bunch interaction and can result in multi-bunch instabilities, whereas the broad-band impedance leads to the intra-bunch particle interaction and can cause single-bunch instabilities.

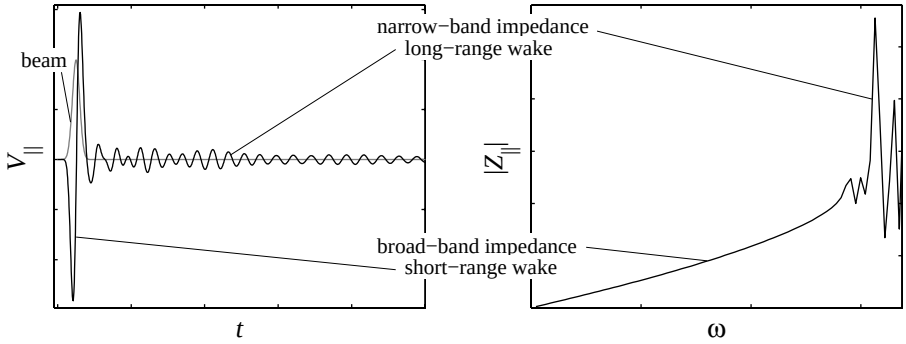

Figure 1: Broad-band and narrow-band impedance.

Broad-band impedance of the vacuum chamber as a whole is a sum of broad-band impedances of all its components. This impedance is generally used as a global criterion of single-bunch beam stability. Since for almost all components of a vacuum chamber, the longitudinal broad-band impedance $Z_{\|}$ is inductive at low frequencies (see Figure 1), it is useful to characterize it in terms of $Z_{\|}$ normalized by the revolution frequency harmonic number $n = \omega/\omega_0$. For a fixed-diameter vacuum chamber with uniformly distributed impedance, there is a relationship between the normalized longitudinal $Z_{\|}/n$ and the transverse dipole $Z_{\perp}$ impedance:

$$\left|Z_{\perp}\right| = \frac{2\,c}{\omega_0 b^2}\left|\frac{Z_{\|}}{n}\right| , \tag{2}$$

where b is the vacuum chamber radius, c is the light speed. If space charge effects are negligible, this formula can be also used as a reference for a non-round vacuum chamber cross-section, in this case b is the average half-size of the chamber.

Impedance of a perfectly conducting chamber results from its cross-section irregularity. For a cylindrical vacuum chamber, there are formulae to estimate low-frequency impedance of an untapered cross-section step from the radius b up to d [4]:

$$\frac{Z_{\|}}{n} = i\frac{\omega_0 Z_0}{2\pi\, c}(d-b)\ln\frac{d}{b} , \qquad Z_{\perp} = i\frac{Z_0}{\pi\, b^2}(d-b)\frac{d^2-b^2}{d^2+b^2} , \tag{3}$$

where $Z_0 \approx 377\ \Omega$ is the free space impedance. These formulae multiplied by factor of 2 can be used for a pill-box cavity with $2(d-b)$ replaced by the cavity length. Tapering with a slope of $\tan\theta$ reduces the impedance roughly by factor of $\sin\theta$.

For a small-angle circular tapered transition of the length l, with the longitudinal shape $r(z)$, there are formulae [5,6] valid at frequencies much less than $\frac{c\,l}{2\pi\,b^2}$:

$$\frac{Z_{\|}}{n} = i\frac{Z_0\omega_0}{4\pi\,c}\int\left(\frac{dr}{dz}\right)^2 dz\ , \qquad Z_{\perp} = -i\frac{Z_0}{2\pi}\int\left(\frac{1}{r}\frac{dr}{dz}\right)^2 dz\ . \tag{4}$$

If the taper is linear, $dr/dz = \tan\theta$, the integrals (4) are standard and the impedance is

$$\frac{Z_{\|}}{n} = i\frac{Z_0\omega_0\tan\theta}{4\pi\,c}(d-b)\ , \qquad Z_{\perp} = i\frac{Z_0\tan\theta}{2\pi}\left(\frac{1}{b}-\frac{1}{d}\right)\ . \tag{5}$$

The impedance of a rectangular taper with the horizontal half-size *h* and the vertical half-size *b* ($h >> b$) is one half of the impedance of a flat tapered collimator [7]:

$$\left(\frac{Z_{\|}}{n}\right)_{\text{rect}} \sim \frac{h}{b}\left(\frac{Z_{\|}}{n}\right)_{\text{circ}}\ , \qquad Z_{\perp} = -i\frac{Z_0 h}{4}\int\frac{1}{r^3}\left(\frac{dr}{dz}\right)^2 dz\ . \tag{6}$$

For the linear taper, the impedance is:

$$Z_{\perp} = i\frac{Z_0 h\tan\theta}{8}\left(\frac{1}{b^2}-\frac{1}{d^2}\right)\ . \tag{7}$$

For a beam stability analysis, there are useful integral factors: the energy loss factor $k_{\|}(0)$, the longitudinal wake gradient $k_{\|}(1)$, and the transverse kick factor $k_{\perp}$. These factors are defined as:

$$k_{\|}(0) = \int_{-\infty}^{\infty} W_{\|}(s)\lambda(s)ds \qquad k_{\|}(1) = -\int_{-\infty}^{\infty}\frac{dW_{\|}(s)}{ds}\lambda(s)ds \qquad k_{\perp} = \int_{-\infty}^{\infty} W_{\perp}(s)\lambda(s)ds\ , \tag{8}$$

where $W_{\|}(s)$ and $W_{\perp}(s)$ are the longitudinal and transverse dipole wake potentials correspondingly, $\lambda(s)$ is the longitudinal beam charge distribution.

4.9.3 Cross-section of the Vacuum Chamber

The vacuum chamber of the damping wiggler section is composed of regular cells with exception of two end cells without absorbers. There are 8 regular cells in one wiggler section, 4 of them have minimal vertical aperture of 9 mm (type "A") and other 4 have this size of 17 mm (type "B"). Coupling impedance of the cells is mainly formed by cross-section transitions between the vacuum chamber fragments. To decrease the impedance, all the fragments are connected by long tapered transitions. Each 6131 mm long regular cell consists of fragments having one of eight different cross-section shapes (see Figure 2). A summary of all the regular cell cross-sections is given in Table 1.

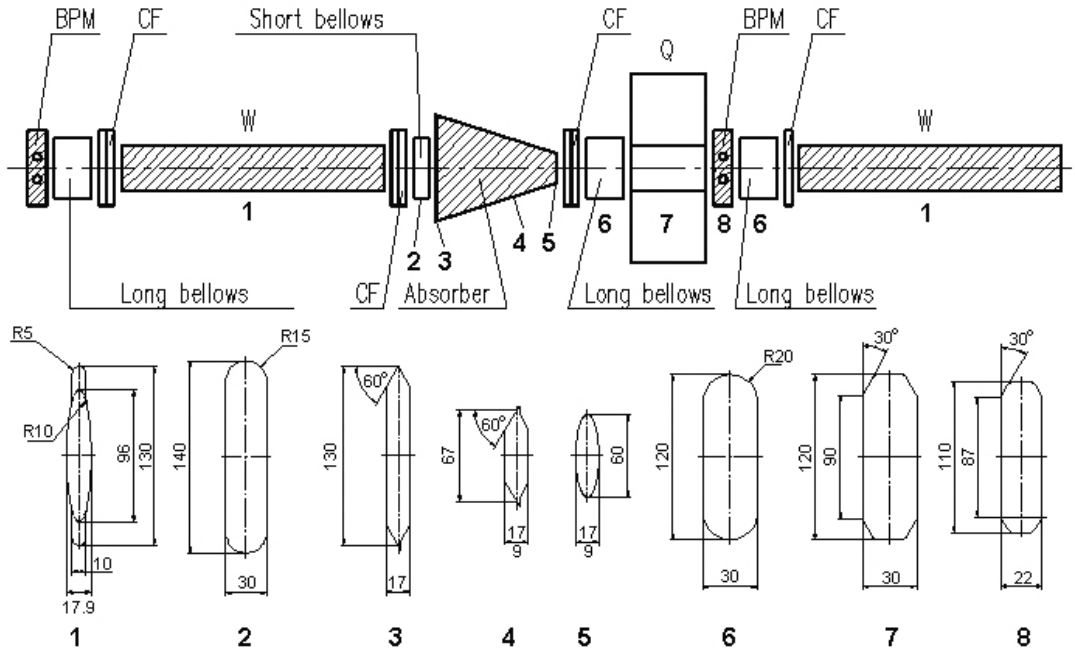

Figure 2: Regular cell of the damping wiggler section.

Table 1: Vacuum chamber cross-sections of the regular cell.

Distance, mm	***Cross-section***	***Aperture,*** hor×ver, mm^2	***Length,*** mm
0	1 (wiggler chamber)	130×17.9	2082
2082	1-2 transition		19.8
2101.8	2 (short bellow)	140×30	84.2
2186	2-3 transition		19
2205	3 (beginning of the absorber)	130×17	0
2205	3-4 transition		500
2705	4 (end of the absorber)	67÷100×9 (A) or 67÷100×17 (B)	0
2705	4-5 transition		160
2865	5 (absorber mask)	60÷96×9 (A) or 60÷96×17 (B)	5
2870	5-6 transition		51.8
2921.8	6 (long bellow)	120×30	118.2
3040	6-7 transition		16
3056	7 (quadrupole)	120×30	740
3796	7-8 transition		20.75
3816.75	8 (BPM mask)	110×20	18.5
3835.25	8-6 transition		20.75
3856	6 (long bellow)	120×30	200
4056	6-1 transition		35
4091	1 (wiggler chamber)	130×17.9	2040

4.9.4 Impedance Budget

To prove reliability of the computer simulations performed using the GdfidL, a cross-check of the GdfidL and MAFIA [8] codes has been carried out. Figure 3 shows an example of the longitudinal (a) and transverse vertical (b) wake potentials calculated using both MAFIA and GdfidL codes for the same cross-section transition 5-6A (see Figure 2 and Table 1). The transition 5-6A is a 51.8 mm-long taper connecting the absorber output with the vertical size of 9 mm and the long bellow with this size of 30 mm. Maximal difference of the MAFIA and GdfidL data is about 0.03 V/pC for the longitudinal wake and 0.05 V/pC for the transverse one, whereas the root-mean-square deviation values are about 0.01 V/pC and 0.02 V/pC correspondingly. Comparative analysis of the GdfidL and MAFIA data allows us to conclude that the GdfidL simulations with the mesh size of 0.5 mm give enough reliable results.

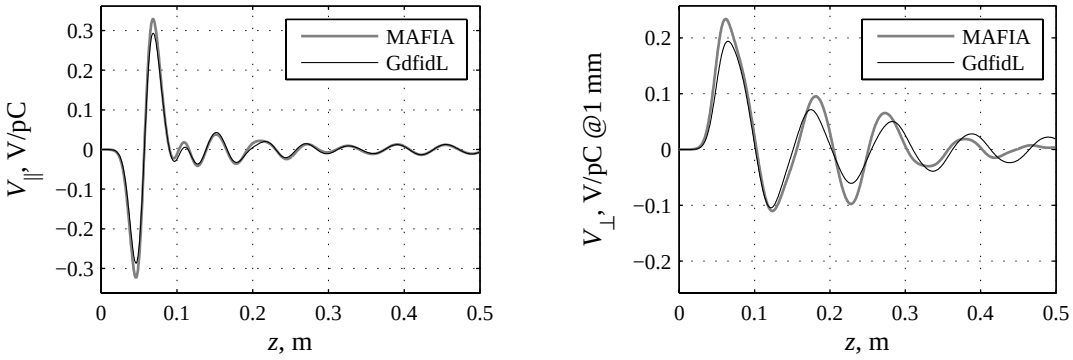

a) **b)**

Figure 3: Cross-check of the GdfidL and MAFIA codes.

For all the cross-section transitions of the regular cells, the longitudinal normalized impedance $Z_{\parallel}/n$, the transverse dipole impedance $Z_{\perp}$ (both horizontal and vertical), and all the integral factors (8) have been calculated using the GdfidL code [2] in comparison with analytical formulae (3)-(7) as a reference.

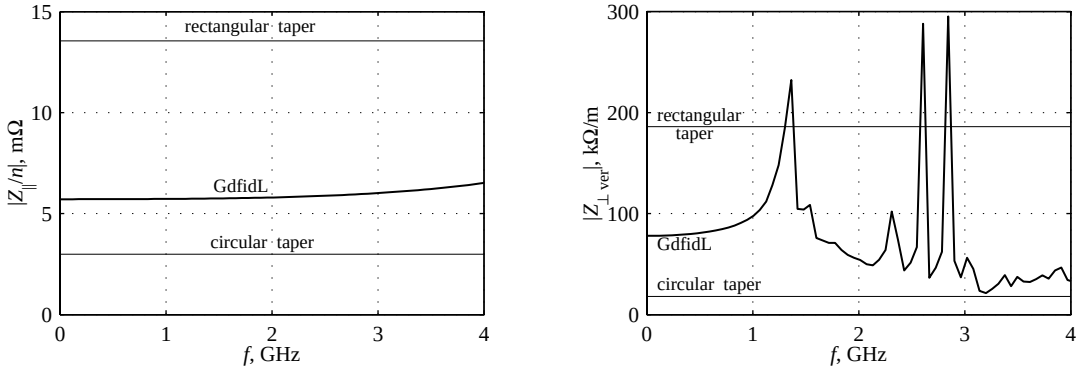

a) **b)**

Figure 4: Longitudinal (a) and transverse vertical (b) impedances of one wiggler section.

Total longitudinal and transverse vertical impedances of one wiggler section, calculated as a sum of impedances of all the cross-section transitions, are presented in Figure 4. There are both the results of the GdfidL simulations performed with the real

geometry, and the rough estimation values calculated using the formulae (4)-(5) for a circular taper, and (6)-(7) for a rectangular one. The energy loss factor $k_{\parallel}(0)$ calculated using GdfidL is about 140 mV/pC, whereas the circular taper formula gives about 70 mV/pC and the rectangular taper formula gives about 330 mV/pC. For the vertical kick factor $k_{\perp \mathrm{ver}}$, these values are 456 V/pC/m, 100 V/pC/m and 1000 V/pC/m correspondingly. One can see that the circular taper approximation gives an underestimate result, whereas the rectangular approximation gives an overestimated one. For short round and rectangular tapers (10 mm long), MAFIA simulations give a quite large difference with the (4)-(7) formulae. The tapers in the wiggler section are probably too short to be treated with the analytic formula. Nevertheless, in many cases the formula (4) multiplied by factor of 3 is a good approximation for the PETRA III tapers.

For all the cross-section transitions, the low-frequency broad-band impedance, loss factor and kick factors are summarized in Table 2. The GdfidL data is used, the low-frequency broad-band impedance is defined as a mean value of the impedance in the 0÷1 GHz frequency band, the kick factors are calculated by numerical integration of the expressions (8). The last three rows of the table show the values related to one cell "A", one cell "B", and one wiggler section including 4 cells "A" and 4 cells "B".

Table 2: Broad-band impedance, loss factor and kick factors summary.

Taper	***Aperture*** hor×ver, mm²	$\lvert Z_{\parallel}/n \rvert$ mΩ	$\lvert Z_{\perp \mathrm{hor}} \rvert$ kΩ/m	$\lvert Z_{\perp \mathrm{ver}} \rvert$ kΩ/m	$k_{\parallel}(0)$ mV/pC	$k_{\parallel}(1)$ V/pC/m	$k_{\perp \mathrm{hor}}$ V/pC/m	$k_{\perp \mathrm{ver}}$ V/pC/m
1-2	130×17.9→140×30	0.151	0.203	1.610	3.406	2.497	1.795	7.455
2-3	140×30→130×17	0.180	0.241	2.334	4.998	3.108	2.139	10.02
3-4A	130×17→80.6×9	0.071	0.407	1.981	0.209	1.287	3.627	17.27
4-5A	80.6×9→60×9	0.000	0.001	0.000	0.000	0.000	0.005	0.001
5-6A	60×9→120×20	0.122	0.534	5.042	0.408	2.040	4.620	31.56
3-4B	130×17→80.6×17	0.000	0.000	0.000	0.000	0.000	0.000	0.000
4-5B	80.6×17→60×17	0.001	0.008	0.001	0.002	0.009	0.071	0.010
5-6B	60×17→120×20	0.021	0.060	0.252	0.080	0.355	0.525	1.714
6-7	120×20→120×30	0.020	0.000	0.188	0.457	0.493	0.000	1.486
7-8	120×30→110×22	0.076	0.089	0.637	3.445	1.401	0.802	3.207
8-6	110×22→120×30	0.075	0.090	0.631	3.446	1.401	0.802	3.199
6-1	120×30→130×17.9	0.106	0.163	1.297	1.426	1.907	1.421	6.393
$\Sigma_{1\ \mathrm{cell\ A}}$		**0.80**	**1.73**	**13.7**	**17.8**	**14.1**	**15.2**	**80.6**
$\Sigma_{1\ \mathrm{cell\ B}}$		**0.63**	**0.85**	**6.95**	**17.3**	**11.2**	**7.56**	**33.5**
$\Sigma_{1\ \mathrm{section}}$		**5.7**	**10.3**	**82.7**	**140.2**	**101.2**	**91.1**	**456.3**

Figure 5 shows fractional contributions of the vacuum chamber fragments to the total low-frequency broad-band impedance of one wiggler section. As it was concluded from the simulations, two wiggler sections make a quite big contribution to the total PETRA III vertical kick factor. Main contribution of the wiggler section kick factor comes from the absorber mask taper situated before the quadrupole section. Reducing of the quadrupole vacuum chamber height decreases contribution of the 5-6 taper

(absorber mask), but, unfortunately, contributions of the 7-8 and 8-6 tapers (BPM mask) increase considerably, so a trade-off solution should be found. Last modification of the vacuum chamber geometry allows us to decrease the vertical kick factor of one wiggler section down to 456 V/pC/m. Thus the kick factor of two wiggler sections is 912 V/pC/m, which is about 20% of the total PETRA III design value.

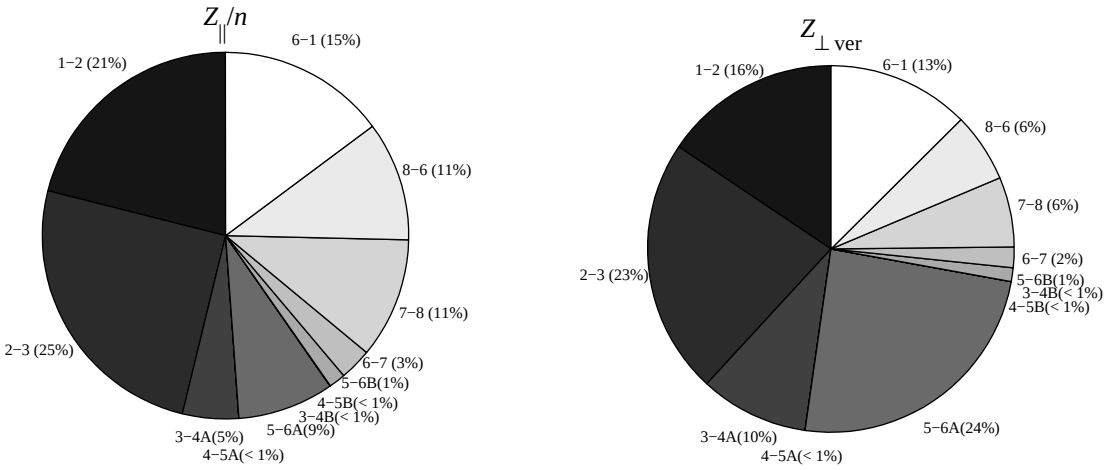

a) **b)**

Figure 5: Impedance contributions: longitudinal (a) and transverse vertical (b).

To protect the PETRA III dipole magnets from synchrotron radiation coming out of the damping wiggler section, an additional mask has been designed to place at the end of the section, between the last quadrupole and the dipole magnet. Coupling impedance of this mask has been estimated using the GdfidL code, to optimize the vertical aperture. A rectangular taper has been taken as the model geometry. The horizontal size of the model is constant of 120 mm, the vertical one decreases from 58 mm (quadrupole) down to the minimum, then it increases up to 38 mm (dipole). The calculations have been done for a set of the minimal aperture values in the 9-22 mm range, the low-frequency broad-band impedance, loss factor and kick factors are presented in Table 3.

Table 3: Broad-band impedance, loss factor and kick factors of the dipole magnet mask.

$2b$ mm	$\lvert Z_{\parallel}/n\rvert$ mΩ	$\lvert Z_{\perp\,\mathrm{hor}}\rvert$ kΩ/m	$\lvert Z_{\perp\,\mathrm{ver}}\rvert$ kΩ/m	$k_{\parallel}(0)$ mV/pC	$k_{\parallel}(1)$ V/pC/m	$k_{\perp\,\mathrm{hor}}$ V/pC/m	$k_{\perp\,\mathrm{ver}}$ V/pC/m
9	1.45	1.49	30.0	47.1	19.3	12.4	127.3
10	1.41	1.23	25.3	46.2	18.6	11.1	108.9
12	1.09	0.85	15.0	40.9	16.4	7.13	63.0
14	0.95	0.68	11.7	37.2	15.1	5.85	49.2
17	0.71	0.46	7.41	32.5	13.1	4.10	31.7
20	0.70	0.30	4.47	29.5	10.8	2.73	19.5
22	0.54	0.24	3.26	27.0	9.41	2.10	14.3

Figure 6 shows the broad-band longitudinal normalized impedance $\lvert Z_{\parallel}/n\rvert$ (a) and the transverse vertical impedance $\lvert Z_{\perp\,\mathrm{ver}}\rvert$ (b) in dependence of the mask vertical

aperture $2b$. The low-frequency broad-band impedance is the impedance calculated by the GdfidL code averaged over the 0÷1 GHz frequency band. The simulation results are presented by the dots, the dashed curves are fits, the solid curves result from analytical impedance estimation using the formulae (6)-(7).

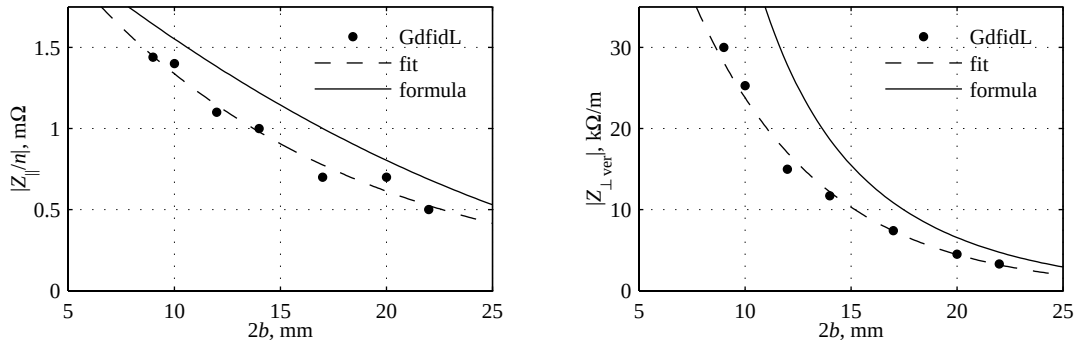

a) **b)**

Figure 6: Longitudinal (a) and transverse vertical (b) impedance vs. vertical aperture.

These simulations show that the mask with 9 mm vertical aperture adds about 33% to the energy loss factor and about 27% to the vertical kick factor of the wiggler section, the 22-mm mask adds about 19% and 3% correspondingly. The mask with a vertical aperture of 17 mm has been chosen to be built.

4.9.5 References

1. K.Balewski, W.Brefeld, W.Decking, H.Franz, R.Rohlsberger, E.Weckert, "PETRA III: A Low Emittance Synchrotron Radiation Source", Technical Design Report, DESY, Hamburg (2004).
2. W.Bruns, The GdfidL Electromagnetic Field Simulator, http://www.gdfidl.de/
3. A.Chao, Physics of Collective Beam Instabilities, Wiley, New York, 1993.
4. A.W.Chao, M.Tigner, Handbook of Accelerator Physics and Engineering, World Scientific, 1998.
5. K.Yokoya, Impedance of Slowly Tapered Structures, CERN SL/90-88 (AP), Geneva, Switzerland, 1990.
6. F.Zimmermann, Collection of Wake-Field Formulae, CERN, Geneva, Switzerland, 2000.
7. G.V.Stupakov, Geometrical Wake of a Smooth Flat Collimator, SLAC-PUB-7167, SLAC, Stanford, USA, 1996.
8. http://www.cst.com/Content/Products/MAFIA/Overview.aspx